MELTING PERFORMANCE ENHANCEMENT OF FERRO-HYDRODYNAMIC CARREAU NON-NEWTONIAN PCM IN POROUS MEDIA
A Geometrical Evaluation

by

Mohsen TALEBZADEGAN [a*], Mojtaba MORAVEJ [b], Ehsanolah ASSAREH [c], and Mohsen IZADI [d]

[a] Department of Mechanical Engineering, Ahvaz Branch, Islamic Azad University, Ahvaz, Iran
[b] Department of Mechanical Engineering, Payame Noor University, Tehran, Iran
[c] Department of Mechanical Engineering, Dezful Branch, Islamic Azad University, Dezful, Iran
[d] Department of Mechanical Engineering, Lorestan University, Khorramabad, Iran

Original scientific paper
https://doi.org/10.2298/TSCI210912016T

In this paper melting of a carreau non-Newtonian PCM in the space between two concentric horizontal tubes, which is partially filled with porous material with different shapes but same area, is investigated numerically. A magnetic source is located in the center of the geometry for melting process of PCM to occur in the presence of ferro-hydrodynamic effects. Porous material is made of Cu that covers the cross-section of the inner tube. In addition, the space between inner and outer tubes is saturated with paraffin-wax PCM. Flow of melted paraffin-wax is considered as a Carreau non-Newtonian, laminar and incompressible flow with viscous dissipation that is evaluated in a specific time interval. Boussinesq approximation is valid for the PCM. Also local thermal equilibrium condition is assumed between the porous and the PCM. Galerkin finite element method has been utilized to solve the problem. Results showed that melting rate is higher for the third model in comparison other models. Also effects of the magnetic number depends on the shape of the porous medium. Therefore, that increase in the magnetic number, increasingly enhances the progress of the melting front in the second case. Moreover, effects of Carreau index, Stefan number, and porosity on the melting process are studied.

Key words: *PCM, porous media, magnetic field, heat transfer enhancement, non-Newtonian fluid*

Introduction

The study of solid-liquid PCM in porous media has received a lot of attention in recent years because of it's vital role in industrial applications, such as solar power collectors, electronics devices, building, computer sciences and heat [1-4]. According to this concept that a small segment of PCM can store a considerable amount of energy during of phase change process. The thermal storage technology is important in the energy saving performance. Gau and Viskanta [5] experimentally reported the effect of natural convection on solid liquid interface move and heat transfer during melting and solidification of gallium on a vertical wall. The authors have investigated the melting interface using a pour-out method and the probing method. Tian and Zhao [6], experimented the effects of Cu foam on heat transfer enhancement on the melting process of paraffin wax RT58. The main finding of their research is that the heat conduction rate is increased

[*] Corresponding author, e-mail: talebzadegan.m@gmail.com

significantly by using metal foams. They found that by adding the metal foam, PCM heat transfer performance is enhanced. Also, their results showed that the metal foams with smaller porosity could have a better heat transfer efficiency as compared to those with larger porosity. Nowadays, non-Newtonian fluid-flow in porous media appears in different fields of engineering application, such as oil recovery, foods and material processing [7-16]. Non-Newtonian fluids in porous media shows a non-linear behavior than the Newtonian one. Ghalambaz *et al.* [17] numerically investigated the impacts of ferro-hydrodynamic (FHD) and MHD on the mass and heat transfer processes of a nanofluid in a hexagonal enclosure. First, momentum equations in horizontal and vertical directions, and the energy equation are obtained and then they were transformed into non-dimensional forms. Results indicated that heat and mass transfer rate goes up with increment of magnetic number. Furthermore, increasing of Hartmann number leads to decline of heat and mass transfer. Izadi *et al.* [18] numerically studied the convective heat transfer in a rectangular enclosure containing porous material under an inclined periodic magnetic field. Governing equations formulated for a single-phase nanofluid and using Darcy-Brinkman with the local thermal non-equilibrium state between fluid and porous material, and in the presence of magnetic field. These equations were solved by Galerkin finite element method (GFEM). They assessed the influences of Darcy number, Hartmann number, Rayleigh number, magnetic field, magnetic field inclination angle and the porosity on the flow pattern and heat transfer. They concluded that the periodic magnetic field has non-uniform effect on the heat transfer process. Ghalambaz *et al.* [19] numerically investigated the melt flow and heat transfer in a PCM in a square cavity under non-uniform magnetic field. Magnetic source is placed near the hot wall. Moving grid method is employed for modelling of the melting process. Results showed that effects of magnetic field on the melting process could be neglected at initial stages. Location of magnetic source affects the melting process, in a way that moving the magnetic source from bottom to middle of the cavity leads to a decrease in required time of melting process. Ghalambaz *et al.* [20] numerically studied the non-Newtonian behavior of MHD and FHD PCM in a rectangular enclosure. A Power-law non-Newtonian fluid is picked as PCM. A non-uniform magnetic field is placed near the hot wall. The top and bottom walls of the enclosure is assumed insulated. Modelling of melting process is performed by moving grid method. They studied the effects of Rayleigh number, Power-law index, Hartmann number, and the magnetic field parameter. Results showed that decreasing of Power-law index increases the melting process. Furthermore, declining of Hartmann number and magnetic parameter give rise to the melt volume fraction.

Model explanation

Figure 1 shows the 2-D section of the two concentric horizontal tubes which the space between is partially filled with porous materials of different shapes but same area. A local magnetic source is placed at the center of the geometry to melting process of PCM occur under influence of FHD. Diameter of inner and outer tubes are D2 and D1, respectively. Difference between temperatures of inner and outer tubes are constant in a way that temperature of inner tube is T_{h} and is higher than temperature of the outer tube T_{c}. Be noted that changes in the PCM thermophysical properties during phase change process are neglected. Physical properties of the porous medium and PCM are given in tab. 1. Paraffin-wax melting flow are considered as incompressible, laminar and Carreau non-Newtonian with viscous dissipation, which is evaluated during a specific time interval. Boussinesq approximation is valid for the melting of PCM. The porous media is made of Cu and covers the axial section of the inner tube. Moreover, the simple and porous space between the two tubes is saturated from paraffin-wax PCM. In addition, local thermal equilibrium condition is assumed to be applied between porous medium and PCM.

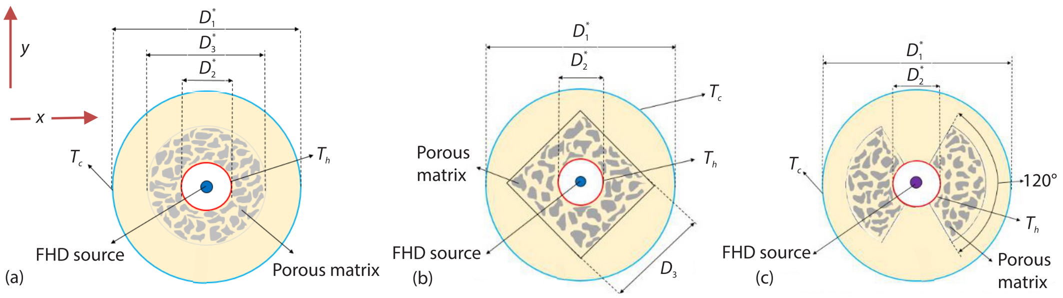

Figure 1. Three physical model with the same areas of porous media; (a) Case 1, (b) Case 2, and (c) Case 3, *PCM – non-Newtonian in liquid phase*

Table 1. Specification of paraffin wax and copper foam [21]

	PCM (Paraffin wax RT58)	Porous medium (copper foam)
Density of solid PCM, ρ_s [kgm^{-3}]	880	8960
Density of fluid PCM, ρ_f [kgm^{-3}]	76	
Volumetric expansion coefficient, β [K^{-1}]	6×10^{-4}	–
Melting temperature, T_f [K]	318-324	–
Thermal conductivity, k [Wm^{-1}K^{-1}]	0.2	401
Latent heat of fusion, L_f [kJkg^{-1}]	168	–
Specific heat in constant pressure, c_p [Jkg^{-1}K^{-1}]	2000	381

Governing equations

To simulate the melting and solidification process of non-Newtonian paraffin wax PCM in double pipe spaces, the enthalpy-porosity method has been employed. Brinkman-Darcy model is also used for porous media. The non-dimensional governing equations for unsteady natural-convection heat transfer of paraffin wax in copper foam and simple media considering the melting and solidification process in the form of continuity, momentum and energy equations [17]:

Continuitu equation:

$$\frac{\partial u}{\partial x}+\frac{\partial v}{\partial y}=0 \tag{1}$$

Momentum equation in x-direction:

$$\begin{gathered}\frac{1}{\varepsilon}\frac{\partial u}{\partial \mathrm{Fo}}+\frac{1}{\varepsilon^2}\left(u\frac{\partial u}{\partial x}+v\frac{\partial u}{\partial y}\right)=-\frac{\partial P}{\partial x}+\frac{\mathrm{Pr}}{\varepsilon}\left(\frac{\partial}{\partial x}(\Omega)\frac{\partial u}{\partial x}+\frac{\partial}{\partial y}(\Omega)\frac{\partial u}{\partial y}\right)-\\ -\frac{\mathrm{Pr}}{\mathrm{Da}}\Omega u+S(\theta)u+Mnf\,\Omega H\frac{\partial H}{\partial y}(\varepsilon_2-\varepsilon_1-\theta)\end{gathered} \tag{2}$$

Momentum equation in y-direction:

$$\begin{gathered}\frac{1}{\varepsilon}\frac{\partial v}{\partial \mathrm{Fo}}+\frac{1}{\varepsilon^2}\left(u\frac{\partial v}{\partial x}+v\frac{\partial v}{\partial y}\right)=-\frac{\partial P}{\partial y}+\frac{\mathrm{Pr}}{\varepsilon}\left(\frac{\partial}{\partial x}(\Omega)\frac{\partial v}{\partial x}+\frac{\partial}{\partial y}(\Omega)\frac{\partial v}{\partial y}\right)-\\ -\frac{\mathrm{Pr}}{\mathrm{Da}}\Omega v+S(\theta)v+Mnf\,\Omega H\frac{\partial H}{\partial y}(\varepsilon_2-\varepsilon_1-\theta)+\mathrm{Ra}\,\mathrm{Pr}\,\theta\end{gathered} \tag{3}$$

Energy equation:

$$\frac{\partial\theta}{\partial \mathrm{Fo}}+\frac{(\rho c_p)_{\mathrm{PCM}}}{(\rho c_p)_{\mathrm{eff}}}\left(u\frac{\partial\theta}{\partial x}+v\frac{\partial\theta}{\partial y}\right)+\varepsilon\frac{(\rho c_p)_{\mathrm{PCM}}}{(\rho c_p)_{\mathrm{eff}}}\frac{1}{\mathrm{Ste}}\left(\frac{\partial\varphi(\theta)}{\partial\tau}\right)=\frac{\alpha_{\mathrm{eff}}}{\alpha_{\mathrm{PCM}}}\left(\frac{\partial^2\theta}{\partial x^2}+\frac{\partial^2\theta}{\partial y^2}\right)+$$
$$+\mathrm{Ec}\Omega Mnf H\left(\theta+\varepsilon_1\right)\left(u\frac{\partial H}{\partial x}+v\frac{\partial H}{\partial y}\right) \tag{4}$$

where:

$$(\rho c_p)_{\mathrm{eff}}=(1-\varepsilon)(\rho c_p)_{\mathrm{porous}}+\varepsilon(\rho c_p)_{\mathrm{PCM}}$$
$$k_{\mathrm{eff}}=(1-\varepsilon)k_{\mathrm{porous}}+\varepsilon k_{\mathrm{PCM}}$$
$$\varphi(\theta)=\begin{cases}0 & \theta<0\\ \dfrac{\theta}{\Delta\theta} & 0<\theta<\Delta\theta\\ 1 & \theta>\Delta\theta\end{cases} \tag{5}$$

$$\alpha_{\mathrm{eff}}=(1-\varepsilon)\alpha_{\mathrm{porous}}+\varepsilon\alpha_{\mathrm{PCM}}$$
$$\Omega=\left\{1+A_{\mathrm{m}}\left[1-\varphi\left(\theta\right)\right]\right\}\left[1+\left(\lambda^*\gamma^*\right)^2\right]^{\frac{n-1}{2}} \tag{6}$$

In equations the non-dimensional parameters are introduced as follows:

$$x=\frac{x^*}{D_1^*},\ y=\frac{y^*}{D_1^*},\ u=\frac{u^*D_1^*}{\alpha_{\mathrm{PCM}}},\ v=\frac{v^*D_1^*}{\alpha_{\mathrm{PCM}}},\ \theta=\frac{T-T_{\mathrm{f}}}{T_{\mathrm{h}}-T_{\mathrm{f}}},\ \mathrm{Da}=\frac{k}{D_1^{*2}}$$
$$\mathrm{Fo}=\frac{t\alpha}{D_1^{*2}},\ p=\frac{p^*D_1^{*2}}{\rho_{\mathrm{PCM}}\alpha_{\mathrm{PCM}}{}^2},\ \gamma=\frac{\gamma^*D_1^{*2}}{\alpha_{\mathrm{PCM}}},\ \lambda=\frac{\lambda^*\alpha}{D_1^{*2}},\ H=\frac{H^*(x^*,y^*)}{H_0^*}$$
$$\mathrm{Pr}=\frac{\mu_{\mathrm{PCM}}}{\rho_{\mathrm{PCM}}\alpha_{\mathrm{PCM}}},\ \mathrm{Ra}=\frac{\mathrm{g}\beta_{\mathrm{PCM}}\Delta TD_1^{*3}}{\upsilon_{\mathrm{PCM}}\alpha_{\mathrm{PCM}}}r,\ \mathrm{Ste}=\frac{c_{p,\mathrm{PCM}}(T_{\mathrm{h}}-T_{\mathrm{f}})}{L_{\mathrm{f}}} \tag{7}$$

$$S(\theta)=-A_{\mathrm{m}}\frac{\left[1-\varphi(\theta)\right]^2}{\varphi^3(\theta)+\varepsilon_p},\ \mathrm{Ec}=\frac{\mu_{\mathrm{PCM}}\alpha_{\mathrm{PCM}}}{\left(\rho c_p\right)_{\mathrm{PCM}}\Delta TD_1^*},\ Mnf=\frac{\mu_0H_0{}^2K'\Delta TD_1^{*2}}{\mu_{\mathrm{PCM}}\alpha_{\mathrm{PCM}}},\ \varepsilon_2=\frac{T_{\mathrm{C}}'}{\Delta T},\ \varepsilon_1=\frac{T_{\mathrm{c}}}{\Delta T}$$

where Pr, Da, Ra, Ste, $\varphi(\theta)$, $(\rho c_p)_{\mathrm{eff}}$, k_{eff}, α_{eff}, ε_1, ε_2, Mnf, Ec, and H are, Prandtl number, Darcy number, Rayleigh number, Stefan number, melting fraction, effective specific heat in constant pressure, effective thermal conductivity coefficient, effective thermal diffuivity coefficient, temperature, Curie temperature, magnetic number, Eckert number, and magnetic field strength.

Dynamic viscosity for Carreau non-Newtonian melting PCM (under melting conditions) can be written [22]:

$$\mu(\gamma)=\mu\left(\varphi\right)\left[1+\left(\lambda\dot{\gamma}\right)^2\right]^{\frac{n-1}{2}},\ \mu\left(\varphi\right)=\mu_{\mathrm{PCM}}\left\{1+A_m\left[1-\varphi(\theta)\right]\right\} \tag{8}$$

The digression of Carreau index from unity depicts the degree of digression from Newtonian behavior that is n = 1 for dilatant fluids. Pseudo-plastic fluids are delineated by an apparent viscosity which descents with ascending shear rate, however in dilatant fluids the apparent viscosity increments with ascending shear rate.

The initial and boundary conditions are also changed in to the non-dimensional from:

$$
\begin{gathered}
u(x,y,0)=0,\ w(x,y,0)=0,\ \text{and}\ \theta(x,y,0)=\theta_{\text{int}} \\
\text{on the inner pipe } -\frac{1}{2}\le x\le\frac{1}{2},\ -\frac{1}{2}\le y\le\frac{1}{2} \\
u\left(x,y,\text{Fo}\right)=0,\ \ w\left(x,y,\text{Fo}\right)=0,\ \text{and}\ \theta\left(x,y,\text{Fo}\right)=1 \\
\text{on the outer pipe } -\frac{1}{2}\le x\le\frac{1}{2},\ -\frac{1}{2}\le y\le\frac{1}{2} \\
u\left(x,y,\text{Fo}\right)=0,\ \text{w}\left(x,y,\text{Fo}\right)=0,\ \text{and}\ \theta\left(x,y,\text{Fo}\right)=0
\end{gathered}
\tag{9}
$$

Effective local and average Nusselt number as well as melting volume fraction defined on the left hot wall of inner pipe and all of the area between two pipes can be written, respectively:

$$
\text{Nu}_{\text{local,eff}}=-\frac{k_{\text{eff}}}{k_{\text{bf}}}\frac{\partial\theta}{\partial n},\text{Nu}_{\text{avg,eff}}=\int_0^1\text{Nu}_{\text{eff}}\text{d}n=-\frac{k_{\text{eff}}}{k_{\text{bf}}}\int_0^1\frac{\partial\theta}{\partial n}\text{d}n,\ \ MVF=\frac{\int_A\phi\left(T\right)\text{d}A}{\int_A\text{d}A}
\tag{10}
$$

Numerical method

The governing equations for the problems introduced in the previous section include PDE with non-linear terms, and so far no analytical method has been presented to solve these equations in general. Governing equations of the problem, including the continuity, momentum, and the energy equation along with the boundary conditions, have been solved by the finite element numerical method. In this study enthalpy-porosity technique employed for the numerical solution of non-Newtonian PCM melting saturated in Cu porous foam. Because in this research, the fixed grid method is used to study the equation, so the grid generation is independent of shape and position of porous medium. Therefore, there is no need to check the grid independence of all cases [21]. On behalf of different cases in this study, the Case 2 is selected to check the independence of grid. A grid independency test has been carried out in order to find the acceptable grid size which will provide exact sufficient answers with a logical computational cost. To check the grid independency of solution, regard to the calculations were repeated for five kinds of uniform triangular networks with sizes 12498, 22464, 32886, 43552, and 54756 for Pr = 50, Ra = $1 \cdot 10^4$, Ste = 0.1, ε = 0.5, *Mnf* = 100, and n = 0.8. The results for different grid sizes and melting volume fraction and average Nusselt number are shown in tab. 2. The conclusions of tab. 2 depict that the grid size of 43552 can provide reasonable precision. Hence, the outcomes of the present research are accomplished using the mesh size 43552.

Table 2. Average Nusselt number, melting volume fraction of the hot inner tube for different uniform grids, Ra = 10000, n = 0.8, Da = 10^{-3}, Ste = 0.1, ε = 0.5, *Mnf* = 100, Fo = 0.001, and **Pr = 50**

Number of element	Process time	Percentage error of melting volume fraction [%]	Percentage error of Nusselt number [%]
12498	6 hour	–	–
22464	9 hour and 40 minutes	0.0025	0.285
32886	12 hour and 42 minutes	0.035	0.265
43552	15 hour and 15 mintes	0.0025	0.545
54756	18 hour and 3 minutes	0.01	0

Validation of computation

To control the accuracy of the solution, three studies have been performed. Altogether, according to the results of the three cases, numerical simulation method of the present research is confirmed with an acceptable accuracy. For the Case 1, fig. 2 depicted a comparison of the local Nusselt number obtained by Sheremet and Pop [23] with current research in two Rayleigh numbers Ra = 100 and Ra = 300. They have studied, natural-convection heat transfer of nanofluid in a triangular cavity filled with porous media. The vertical wall was considered at higher temperature and local Nusselt number evaluated on this wall. They have reported effect of thermophoresis and Brownian motion on the nanofluid. Also, thermal equilibrium model was considered. As can be seen in fig. 2, the results of the current study have good agreement with the results of Sheremet and Pops [23] work. In fig. 3, results of the present study are compared with experimental data of Gau and Viskanta [5]. The comparison is made for enclosure filled with PCM of Gallium and aspect ratio of 0.5. The left wall is assumed hot and the right wall is the cold one. The horizontal walls are insulated. Stefan, Prandtl and Rayleigh numbers are considered 0.04, 0.02, and $6 \cdot 10^5$, respectively. Figure 3 shows that there is good agreement between the results of the present study and experimental data reported by Gau and Viskanta [5]. In the Case 3, fig. 4, a numerical model confirmation for horizontal shell and tube with the partial porous inserts was carried out by Xu *et al.*

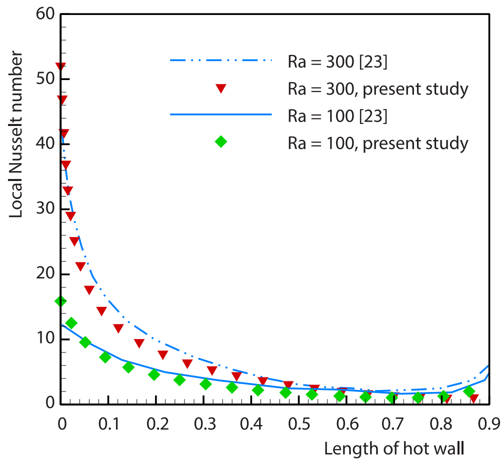

Figure 2. comparison of the local Nusselt number obtained by [23]

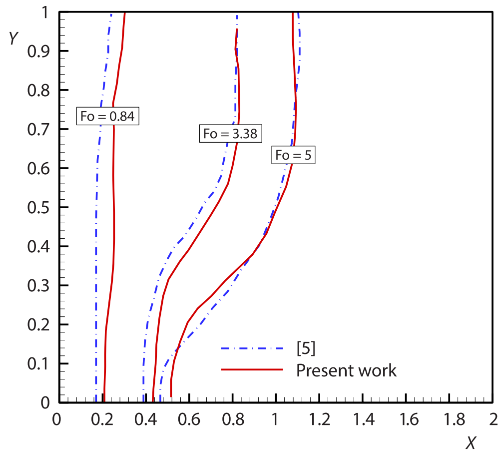

Figure 3. A comparison of the results of the present study with results of laboratory research present study [5]

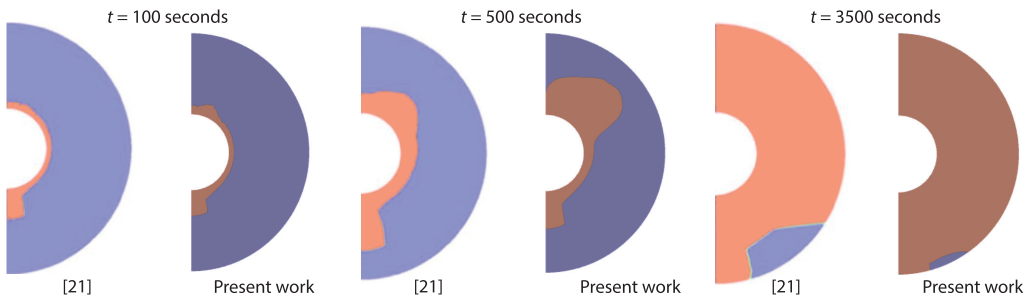

Figure 4. A comparison of the melting fraction in the full porous medium *vs.* obtained results by [21]

[21]. In that study a cross-section of two concentric tubes is considered. The porous inserts has a central angle of 30° of sector-ring shape with 0.8 porosity. The lithium carbonate and Cu foam as a PCM and porous media materials. The inner tube is considered at higher temperature than the outer tube. Comparison have been done for the melting fraction of lithium carbonate at times of 100 secons, 500 seconds, and 3500 secons. It can be found from fig. 4 that there is a good compatibility between the conclusions of the present simulation and the outcomes of Xu *et al.* [21].

Outcomes and discussion

According to the model described in previous section (second section, model explanation) simulation of the melting process of a Carreau non-Newtonian PCM in a part of transverse section of two concentric tubes is performed. This study aims to determine the effects of the shape of porous medium and different parameters on the progress and pattern of the melting front. Results are obtained for the default values of n = 0.8, ε = 0.5, Pr = 50, *Mnf* = 100, Ra = 10^4, and Ste = 0.1. Melting volume fraction variations with non-dimensional time from 0-0.25 for the three mentioned cases with the default values are plotted in fig. 5. As it is clear, at the same times melting volume fraction for the third model is higher than the second model, followed by the first model. Therefore, effects of porous medium can be variable in different geometries but same area. Figure 6 represents streamlines, isotherms and melting volume fraction of PCM at three non-dimensional time (Fo = 0.0005, 0.1, and 0.25) for three different cases. Isotherms are illustrated in the left part of the geometry, and streamlines and melting fraction are plotted in the right part. As it can be seen, condition and shape of the porous medium have significant effects on the value and pattern of the melting fraction, streamlines and isotherms. At the early times, which PCM is in the porous medium, the dominant heat transfer mode is conduction and the impact of natural-convection heat transfer in the porous section is less significant for three cases. So melting front leaves the porous medium at early stages. However, later, when the PCM enters the simple space, the dominant heat transfer mode is natural-convection, which augments the fluid circulation in the annulus region. Results shown in fig. 6 are in agreement with those in fig. 5. As it is obvious, melting amount for the third case is more than the first and second cases. In fact, melting front, extent of streamlines and isotherms at the latest time for the circular segment shape porous medium is higher than the diamond and circular porous medium.

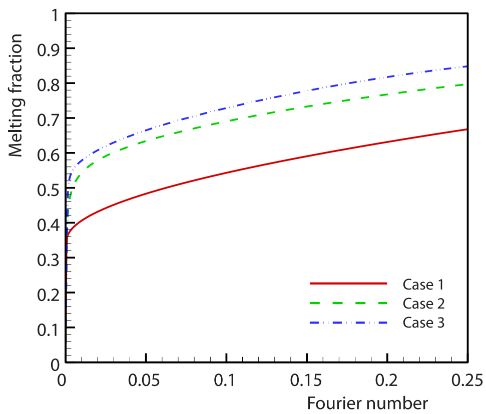

Figure. 5. Comparison of the melting fraction for different Fourier number in default values; (a) Fo = 0.0005, (b) Fo = 0.1, and (c) Fo = 0.25

Impact of magnetic field on the melting process

Effects of the point magnetic field on the melting fraction of PCM for the mentioned three different cases are illustrated in fig. 7 for non-dimensional time from 0-0.25. As it is shown in fig. 7(a), without point magnetic field (*Mnf* = 0) the melting fraction are close for three cases, especially at early times. However, with advancing in time the curve corresponding to the third case deviate from other two curves and represents higher melting fraction. In fact,

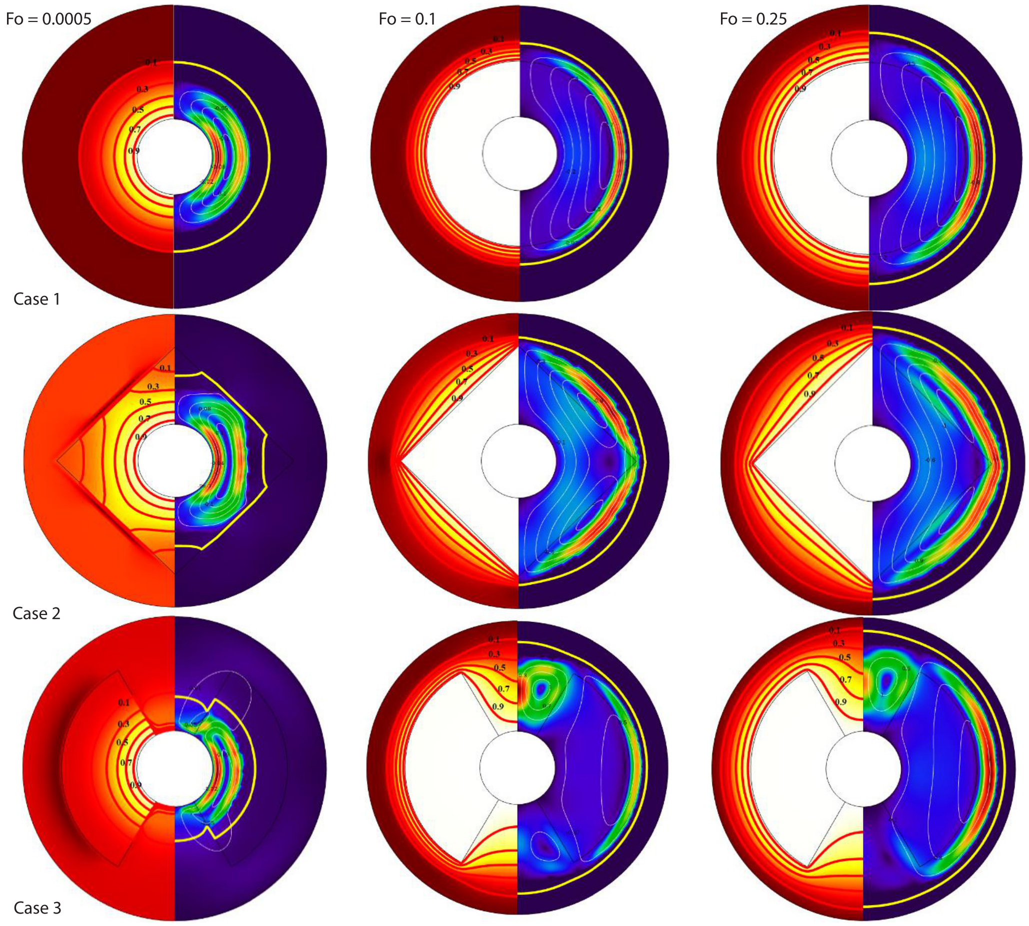

Figure. 6. Evaluation of the contour of isotherms (left side), streamlines and melting fraction front (right side) for three cases in default values for different Fourier number

without point magnetic field at the center of the inner tube, the pattern of the melting fraction in fig. 7(a), is formed by the shape of the porous medium. In the presence of point magnetic field at the center of the inner tube, fig. 7(b), and considering electromagnetic stresses (Kelvin force) and adiabatic cooling (magnetocaloric effect) in the form of magnetic number, progress of melting front in the first case is almost unchanged and in the second and third cases have ascending trends. Therefore, it can be concluded that the presence of the local magnetic field can have positive or negative impacts on the progress of the melting front, depending on the shape of the porous medium. Increasing of the local magnetic field strength in the form of increasing in the magnetic number is illustrated in fig. 7(b). As it can be observed, curve corresponding to the first case is still independent of presence of the magnetic field and its strength. Increasing of the strength of magnetic field has negligible effect on the progress of the melting front in the third case. While the second case affected by the increase in strength of the magnetic field has more progressed melting front in a way that at most of the non-dimensional times, the curve for the second case is located higher or equal to the third case's curve. Hence, overall it can be deduced that effectiveness of the magnetic number on the melting front progress, is dependent on the geometry of the porous medium and strength of the local magnetic field.

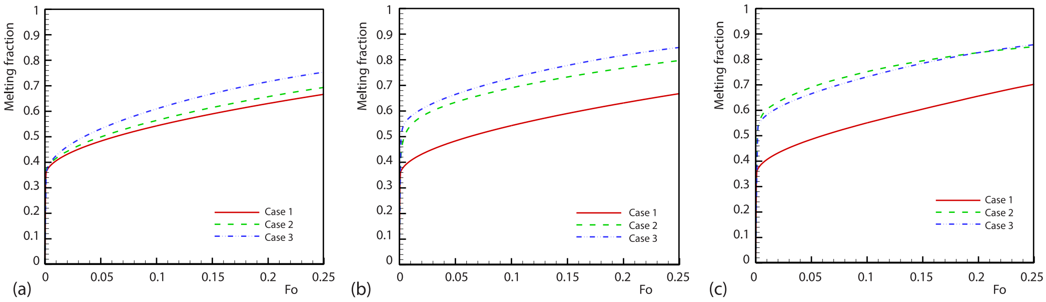

Figure 7. Evaluation of the melting fraction for different magnetic field in default values; (a) *Mnf* = 0, (b) *Mnf* = 100, and (c) *Mnf* = 500

Impact of porosity index on the melting process

Figure 8 shows melting fraction for the three mentioned cases in different values of porosity in the non-dimensional time interval 0-0.25. Since melting process occurs quickly in the porous mediums and majority of impacts of the porosity is in the porous medium, the horizontal axis is considered in logarithmic scale. With increasing of porosity the porous medium between hot and cold tubes tends to be a simple medium. A simple medium (without the porous solid matrix made of Cu foam) has lower conductivity than the porous one. Therefore, at higher values of porosity the conduction mode of heat transfer at early stages is weaken that leads to decrement of melting fraction for all the three cases. However, with declining of porosity on one hand the void volume decreases and on the other hand conductivity of porous medium enhances. Hence, at early stages the melting process of PCM for all the three cases is a strong function of porous medium conductivity, and the lowest value of the porosity results in more melting of the PCM. According to fig. 8 it can be concluded that the effect of the three porous mediums continue to be present to times less than 10^{-3} for $\varepsilon = 0.3$, to time of 10^{-3} for $\varepsilon = 0.5$ and until times beyond 10^{-3} for $\varepsilon = 0.7$. Also for all the cases, range of variations of melting fraction is extended at higher value of porosity. Thereby, the jump in the curve corresponding to $\varepsilon = 0.7$ is more than those corresponding to $\varepsilon = 0.5$ and $\varepsilon = 0.3$. On the other hand for all the specified values of porosity, melting processes for Cases 1 and 2 are almost identical at the early stages. While for the third case as $\varepsilon = 0.3$ is close to other two curves and for $\varepsilon = 0.5$ and $\varepsilon = 0.7$ makes some distance from other two curves. However, after passing the porous medium and entering the simple medium, the third case always has the maximum value of the melt. Therefore, it can be concluded that effects of the porous medium is solely present at early stages and after the melting front enters the simple space the final value of melting fraction at the last time remains unchanged.

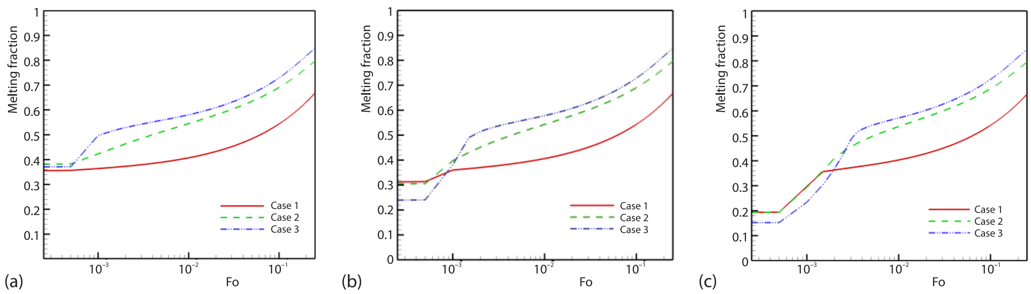

Figure 8. Assessment of melting fraction for different porosity in default values; (a) ε = 0.3, (b) ε = 0.5, and (c) ε = 0.7

Impact of Carreau index on the melting process

Melting fraction of the non-Newtonian PCM in the non-dimensional time interval zero to 0.25 for different carreau index, $n = 0.8$, 1, and 1.2, is derived and plotted in fig. 9. As it can be seen for all the three cases, the Carreau index has insignificant effect on the melting front. So, according to the defined conditions, pseudoplastic non-Newtonian fluid ($n = 0.8$), Newtonian fluid ($n = 1$), and dilatant non-Newtonian fluid ($n = 1.2$) have no significant influence on the melting fraction in all the cases. In fact, in each case after melting of the PCM and progressing of the developed melting front, strengthening or weakening of the shear stress in the melt of the PCM do not lead to increase or decrease in melting velocity. However, it can be expected that the circulation velocity of the melt of the PCM is affected and for the thinning non-Newtonian fluid ($n = 0.8$) more strong streamlines and velocity is developed. Therefore, melting of paraffin wax has the same melting fraction either with Newtonian or non-Newtonian behavior.

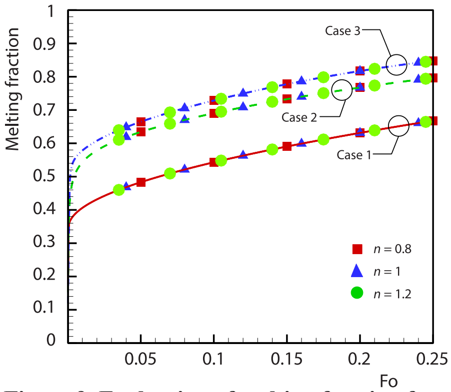

Figure 9. Evaluation of melting fraction for different Carreau index, *n*, in default values

Impact of Stefan number on the melting process

Effects of the Stefan number on the melting fraction of the PCM are illustrated in fig. 10. Increase in Stefan number increases the temperature difference between the inner hot tube, T_h, and the melting point of the PCM, T_f. Therefore, with an increase of Stefan number from 0.05-0.2, in both porous and simple mediums, progressing of the melting fraction of the PCM increases for all the three cases. For Stefan numbers of 0.05 and 0.1 slopes of the three curves rise and in other word melting front maintain its ascending trend until the last time. However, for the Stefan number of 0.2, increase in the melting front progress are ceased after non-dimensional time of 0.2 and the curves reach a plateau. Therefore, it can be concluded that increasing of the Stefan number to beyond 0.2, or in the other word increasing of temperature difference between inner tube and melting point of the PCM, the final melting fraction for the three curves are the same as in fig. 10(c), and only the maximum melting fraction is achieved sooner.

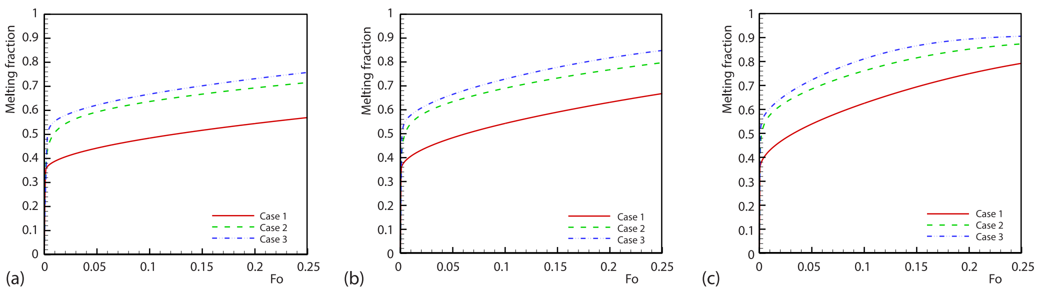

Figure 10. Assessment of melting fraction for different Stefan numbers in default values; (a) Ste = 0.05, (b) Ste = 0.1, and (c) Ste = 0.2

Conclusions

Melting process of the paraffin-wax PCM in the annulus between two concentric tubes are studied using the enthalpy-porosity method. The annulus is partially filled with porous material. Effects of FHD due to the presence of a local magnetic field at the center of the inner tube are investigated. Paraffin wax after melting shows non-Newtonian behavior and is assumed in the local thermal equilibrium conditions with the solid porous matrix. By considering three different shape for the porous medium (circular, diamond, circular sector), the main findings of the present study are as follows.

- Effects of the magnetic number depends on the shape of the porous medium. Kelvin force and magnetocaloric effect have the most impact on the Case 2. Therefore, that increase in the magnetic number, increasingly enhances the progress of the melting front in the Case 2. When circular porous medium (Case 1) is used, presence of the magnetic field has no effects on the melting fraction. In addition, increase in magnetic field has a limited effect on the progress of the melting fraction of paraffin wax and this case shows no response to the high increasing of the magnetic number.
- Porosity affects the melting fraction of the PCM only in the porous medium. Increase in porosity make the porous medium approach a simple one. By raising the porosity, Cases 1 and 2 decreases almost identical along to each other. However, maximum decrement occurs for the third case.
- Paraffin wax as an pseudoplastic non-Newtonian fluid with carreau index of $n = 0.8$, Newtonian fluid with $n = 1$, and dilatant non-Newtonian fluid with $n = 1.2$ has no effect on the melting process.
- Stefan number in all the annulus space (medium and simple medium) has positive effects on the melting fraction of the PCM for all the three cases. Increase in the temperature difference between the hot surface of the inner tube and melting point of the PCM leads to the quick melting of the paraffin wax. At all the specified values for the Stefan number, the Case 3 (porous medium with circular sector geometry) is above the Case 2 (diamond porous medium) following by the Case 1 (circular porous medium).

Nomenclature

A_m – Mushy-Zone constant, [kgm^{-3}s^{-1}]
c_p – specific heat in constant pressure[Jkg^{-}1K^{-1}]
Da – Darcy number, [–]
Ec – Eckert number, [–]
Fo – Fourier number, [–]
g – gravity, [ms^{-2}]
H – magnetic field strength, [Am^{-1}]
k – thermal conductivity, [Wm^{-1}K^{-1}]
K' – constant parameter, [–]
L_f – latent heat of fusion, [Jkg^{-1}]
Mnf – magnetic number, [–]
n – Carreau index
P – pressure, [Pa]
Pr – Prandtl number, [–]
Ra – Rayleigh number, [–]
Ste – Stefan number, [–]
$S(t)$ – Carman-Kozeny equation (source term)
T – dimensional temperature, [K]
T'_C – Curie temperature, [–]
T_c – cold temperature, [K]
T_f – melting temperature, [K]
T_h – hot temperature, [K]
t – time, [second]
u^* – velocity in the x-direction [ms^{-1}]
v^* – velocity in the y-direction, [ms^{-1}]
X – Cartesian component in horizontal direction, [m]
Y – Cartesian component in vertical direction, [m]

Greek symbols

α – thermal diffusivity, [m^{2}s^{-1}]
β – volumetric expansion coefficient, [K^{-1}]
ε – porosity, [–]
ε_1 – temperature number, [–]
ε_2 – Curie temperature number, [–]
ε_p – Carman-Kozeny equation constant, [–]
θ – non-dimensional temperature, [–]
λ – time dependent parameter, [s]
ρ_s – density of solid PCM, [kgm^{-3}]
ρ_f – density of fluid PCM, [kgm^{-3}]

References

[1] Kandasamy, R., *et al*., Transient Cooling of Electronics Using Phase Change Material (PCM)-Based Heat Sinks, *Applied Thermal Engineering*, *28* (2008), 8, pp. 1047-1057

[2] Tan, W. C., *et al*., Overview of Porous Media/Metal Foam Application in Fuel Cells and Solar Power Systems, *Renewable and Sustainable Energy Reviews*, *96* (2018), Nov., pp. 181-197

[3] Parameshwaran, R., Kalaiselvam, S., Energy Efficient Hybrid Nanocomposite-Based Cool Thermal Storage Air Conditioning System for Sustainable Buildings, *Energy*, *59* (2013), Sept., pp. 194-214

[4] Nomura, T., *et al*., Heat Storage in Direct-Contact Heat Exchanger with Phase Change Material, *Applied Thermal Engineering*, *50* (2013), 1, pp. 26-34

[5] Gau, C., Viskanta, R., Melting and Solidification of a Pure Metal on a Vertical Wall, *Journal Heat Trans*., *108* (1986), 1, pp. 174-181

[6] Tian, Y., Zhao, C.-Y., A Numerical Investigation of Heat Transfer in Phase Change Materials (PCM) Embedded in Porous Metals, *Energy*, *36* (2011), 9, pp. 5539-5546

[7] Adhikari, B., Jindal, V., Artificial Neural Networks: A New Tool for Prediction of Pressure Drop of Non-Newtonian Fluid Foods through Tubes, *Journal of Food Engineering*, *46* (2000), 1, pp. 43-51

[8] Mehryan, S., *et al*., Non-Newtonian Phase Change Study of Nanoenhanced n-Octadecane Comprising Mesoporous Silica in a Porous Medium, *Applied Mathematical Modelling*, *97* (2021), Sept., pp. 463-482

[9] Kebriti, S., Moqtaderi, H., Numerical Simulation of Convective non-Newtonian Power-Law Solid-Liquid Phase Change Using the Lattice Boltzmann Method, *International Journal of Thermal Sciences*, *159* (2021), 106574

[10] Chen, H.-T., Natural-Convection of a non-Newtonian Fluid about a Horizontal Cylinder and a Sphere in a Porous Medium, *International Communications in Heat and Mass Transfer*, *15* (1988), 5, pp. 605-614

[11] Qi, C., *et al*., Effects of Rotation Angle and Metal Foam on Natural-Convection of Nanofluids in a Cavity under an Adjustable Magnetic Field, *International Communications in Heat and Mass Transfer*, *109* (2019), 104349

[12] Mehryan, S., *et al*., Melting Behavior of Phase Change Materials in the Presence of a non-Uniform Magnetic-Field Due to Two Variable Magnetic Sources, *International Journal of Heat and Mass Transfer*, *149* (2020), 119184

[13] Izadi, M., *et al*., Location Impact of a Pair of Magnetic Sources on Melting of a Magneto-Ferro Phase Change Substance, *Chinese Journal of Physics*, *65* (2020), June, pp. 377-388

[14] Mehryan, S., *et al*., Natural-Convection of Multi-Walled Carbon Nanotube-Fe_3O_4/Water Magnetic Hybrid Nanofluid-Flowing in Porous Medium Considering the Impacts of Magnetic Field-Dependent Viscosity, *Journal of Thermal Analysis and Calorimetry*, *138* (2019), 2, pp. 1541-1555

[15] Kefayati, G. R., The FDLBM Simulation of Magnetic Field Effect on Mixed Convection in a Two Sided Lid-Driven Cavity Filled with non-Newtonian Nanofluid, *Powder Technology*, *280* (2015), Aug., pp. 135-153

[16] Mehryan, S., *et al*., Natural-Convection and Entropy Generation of a Ferrofluid in a Square Enclosure under the Effect of a Horizontal Periodic Magnetic Field, *Journal of Molecular Liquid*s, *263* (2018), Aug., pp. 510-525

[17] Ghalambaz, M., *et al*., Insight into the Dynamics of Ferrohydrodynamic (FHD) and Magnetohydrodynamic (MHD) Nanofluids Inside a Hexagonal Cavity in the Presence of a non-Uniform Magnetic Field, *Journal of Magnetism and Magnetic Materials*, *497* (2020), 166024

[18] Izadi, M., *et al*., Natural-Convection of a Hybrid Nanofluid Affected by an Inclined Periodic Magnetic Field within a Porous Medium, *Chinese Journal of Physics*, *65* (2020), June, pp. 447-458

[19] Ghalambaz, M., *et al.*, Analysis of Melting Behavior of PCM in a Cavity Subject to a non-Uniform Magnetic Field Using a Moving Grid Technique, *Applied Mathematical Modelling*, *77 Part 2* (2020), Jan., pp. 1936-1953

[20] Ghalambaz, M., *et al*., Non-Newtonian Behavior of an Electrical and Magnetizable Phase Change Material in a Filled Enclosure in the Presence of a non-Uniform Magnetic Field, *International Communications in Heat and Mass Transfer*, *110* (2020), 104437

[21] Xu, Y., *et al*., Evaluation and Optimization of Melting Performance for a Latent Heat Thermal Energy Storage Unit Partially Filled with Porous Media, *Applied Energy*, *193* (2017), May, pp. 84-95

[22] Bird, R. B., *et al*., Dynamics of Polymeric Liquids, in: *Fluid Mechanics*, Vol. 1, Willy, New York, USA, 1987

[23] Sheremet, M. A., Pop, I., Free Convection in a Triangular Cavity Filled with a Porous Medium Saturated by a Nanofluid, *International Journal of Numerical Methods for Heat and Fluid-Flow*, *25* (2015), 5, pp. 1138-1161

Paper submitted: September 12, 2021
Paper revised: November 18, 2021
Paper accepted: November 20, 2021